Journal Name

ARTICLE

Microstructures of negative and positive azeotropes†

J. J. Shephard,[a, b] S. K. Callear,[c] S. Imberti,[c] J. S. O. Evans[b] and C. G. Salzmann*[a]

Received 00th January 20xx,
Accepted 00th January 20xx

DOI: 10.1039/x0xx00000x

www.rsc.org/

Azeotropes famously impose fundamental restrictions on distillation processes, yet their special thermodynamic properties make them highly desirable for a diverse range of industrial and technological applications. Using neutron diffraction, we investigate the structures of two prototypical azeotropes, the negative acetone-chloroform and the positive benzene-methanol azeotrope. C–H···O hydrogen bonding is the dominating interaction in the negative azeotrope but C–Cl···O halogen bonding contributes as well. Hydrogen-bonded chains of methanol molecules, which are on average longer than in pure methanol, are the defining structural feature of the positive azeotrope illustrating the fundamentally different local mixing in the two kinds of azeotropes. The emerging trend for both azeotropes is that the more volatile components experience the more pronounced structural changes in their local environments as the azeotropes form. The mixing of the acetone-chloroform azeotrope is essentially random above 20 Å where the running Kirkwood-Buff integrals of our structural model converge closely to the ones expected from thermodynamic data. The benzene-methanol azeotrope on the other hand displays extended methanol-rich regions and consequently, the running Kirkwood-Buff integrals oscillate up to at least 60 Å. Our study provides first insights into the microstructures of azeotropes and a direct link with their thermodynamic properties. Ultimately, this will provide a route for creating tailored molecular environments in azeotropes to improve and fine-tune their performances.

Introduction

Azeotropes are mixtures of liquids whose vapour has the same composition as the liquid phase.[1-4] They form at the limit of fractional distillation where it becomes impossible to achieve further separation of the components as equal amounts evaporate at a sharply defined boiling point. Azeotropes therefore have some thermodynamic properties more characteristic of pure, single-component liquids. Whilst azeotropes impose fundamental restrictions on purification processes, their thermodynamic properties are highly desirable for a wide range of applications. Azeotropic cleaning fluids, for example, remain constant in their composition during application, and can be recovered at the original composition by vaporisation and recondensation.[5] Furthermore, flammable but otherwise functional liquids can be formulated in a safe and stable fashion as inflammable azeotropes.[5] Finally, azeotropes can release defined and constant amounts of an anaesthetic component into the gas phase.[6]

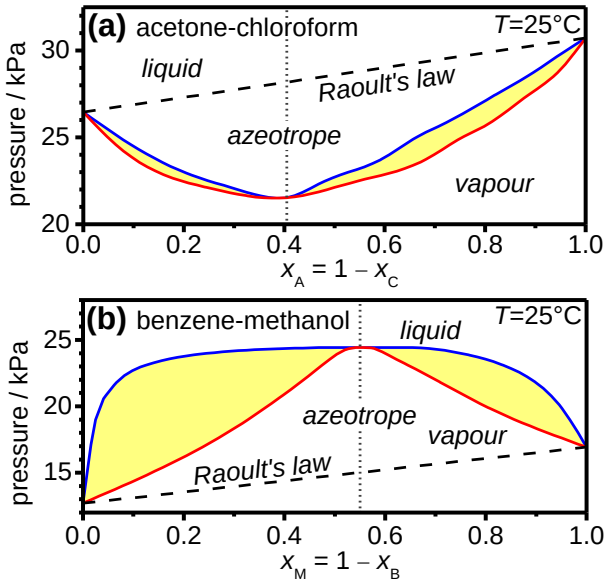

Figure 1 Pressure-composition phase diagrams of (a) acetone-chloroform[7, 8] and (b) benzene-methanol[9] at 25°C. The azeotropic compositions are indicated by dotted vertical lines at x_A=0.405 and x_M=0.550, respectively. The dashed lines indicate ideal behaviour according to Raoult's law and the yellow areas highlight the two-phase regions.

Azeotropy is fundamentally linked with strong deviations from the behaviour of ideal mixtures for which the enthalpy of mixing is zero and the total vapour pressure follows the linear trend described by Raoult's law.[1-3] The acetone-chloroform azeotrope is a popular text book example of a negative or maximum-boiling azeotrope displaying negative deviations from Raoult's

[a] *Department of Chemistry, University College London, 20 Gordon Street, WC1H 0AJ London, UK. Email: c.salzmann@ucl.ac.uk*
[b] *Department of Chemistry, Durham University, South Road, Durham DH1 3LE, UK.*
[c] *ISIS Facility, Rutherford Appleton Laboratory, Didcot, OX11 0QX, UK.*

† Electronic Supplementary Information (ESI) available: Materials; Neutron scattering experiments; Empirical Potential Structural Refinement; Classification of local environments in the EPSR models; X-ray diffraction and differential scanning calorimetry upon cooling; Calculation of Kirkwood-Buff integrals from thermodynamic data. See DOI: 10.1039/x0xx00000x

law, as shown in Figure 1(a), as well as an exothermic enthalpy of mixing.[7, 8, 10-18] The non-ideality of acetone-chloroform mixtures is often attributed to the formation of C–H···O hydrogen bonds between chloroform and acetone. In fact, this system was one of the first for which a hydrogen bond with a C–H donor was proposed.[19]

Conversely, the benzene-methanol system is a positive or minimum-boiling azeotrope with an endothermic enthalpy of mixing.[9, 20, 21] The positive deviations from Raoult's law indicate weaker benzene-methanol interactions relative to stronger benzene-benzene and methanol-methanol interactions (Figure 1(b)). Only about 1% of azeotropes are negative and positive azeotropes are therefore far more frequently encountered.[22] It is generally difficult to predict if two liquids will form an azeotrope. Yet, the existence of a Bancroft point, which is defined by the temperature and pressure where the vapour pressures of the two pure components are the same, is typically a very strong indicator.[2, 23]

Despite the general importance of azeotropes relatively little is known about their microstructures. Acetone-chloroform mixtures have been studied, although not always at the azeotropic composition, by analysis of thermodynamic excess functions, [7, 8, 10-18] NMR,[24-27] Raman,[28, 29] FT-IR,[27, 28, 30] NIR,[31] terahertz time-domain[32] and inelastic neutron spectroscopy[29] as well as Monte Carlo simulations.[22] There is general consensus that hydrogen bonding interactions are likely to be present. For example, a peak at 82 cm^{-1} in the inelastic neutron spectrum has been assigned to the *anti*-translational mode of the 1:1 hydrogen bonded complex.[29] Yet, in summary, the strength, prevalence and geometries of the hydrogen bonds are not well understood.

The benzene-methanol system is also not well understood. Based on differences in Raman shifts upon forming the azeotrope, complexation between benzene and methanol has been suggested to occur.[33] However, in light of the known tendency of methanol to self-associate through hydrogen bonding[34-38] and the positive enthalpy of mixing,[20] such complexes, if present, are not expected to contribute significantly to the azeotropic behaviour. A study carried out by Ploetz *et al.* provided a different viewpoint on azeotrope formation in this system.[39] Using Kirkwood-Buff integrals[40] they found a large positive value for the integral describing methanol-methanol pairs in benzene-rich mixtures. This indicates the aggregation of methanol molecules and that the mixture approaches heterogeneous phase separation.[41, 42]

Here we investigate the origins of azeotropy from a structural point of view. We use the Empirical Potential Structure Refinement (EPSR) approach[43, 44] in combination with neutron diffraction measurements and the isotopic substitution technique to obtain structural models representative of acetone-chloroform and benzene-methanol azeotropes. In addition to investigating the local molecular environments in these azeotropes we gain information about the more long-range state of mixing using Kirkwood-Buff integrals derived from both the structural models and from thermodynamic data. Using the two classic examples of positive and negative azeotropes we finally aim to describe general structural trends caused by the appearance of the two different types of azeotropy.

Results and discussion

Empirical Potential Structural refinement

Using the EPSR approach[43, 44] we obtained three-dimensional structural models of the two azeotropes which are in agreement with the experimental neutron diffraction data shown in Figure 2. Fitting the diffraction data of several isotopically different mixtures greatly increases the reliability of the structure reconstruction process. The convergence of the measured and simulated diffraction data is achieved by EPSR by optimising so-called empirical potentials which are defined between all the intermolecular atom pairs. Further details on EPSR and the isotopic substitution technique are given in the ESI.

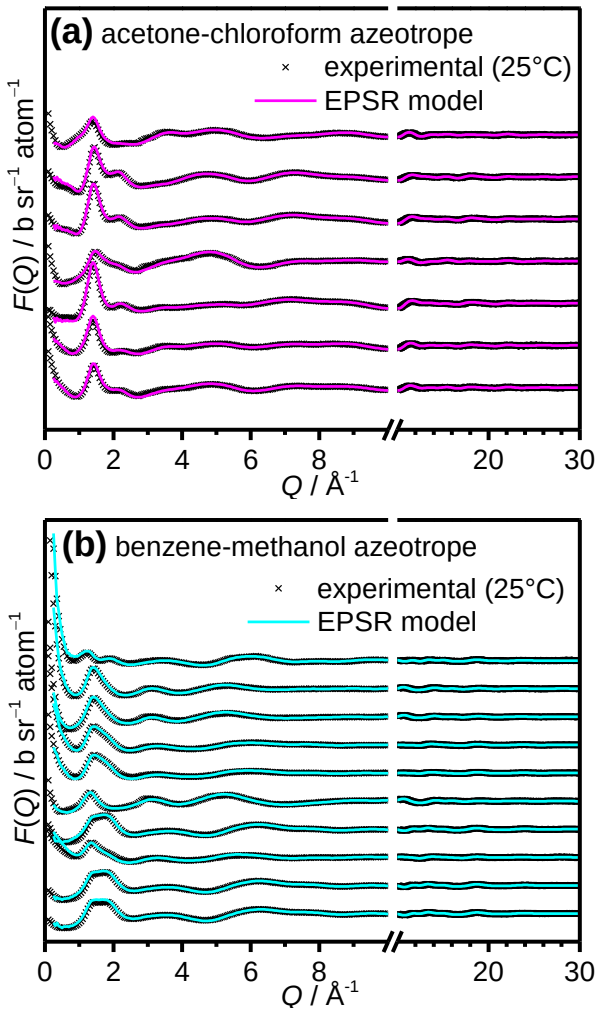

Figure 2 Experimental (crosses) and simulated neutron diffraction data (lines) for a series of isotopically different (a) acetone-chloroform and (b) benzene-methanol azeotropes. The datasets (a) and (b) are offset vertically in order of increasing scattering length density contrast. The isotopic compositions of the various samples are given in the ESI.

Creating structural models which represent the structure over sufficiently large distances to be thermodynamically accurate is

one of the main challenges in the study of non-ideal mixtures which tend towards molecular aggregation. To tackle this issue, we use quite large simulation boxes (~120×120×120 Å) which minimise the reliance on periodic boundary conditions and allows structurally representative aggregations to form within the simulation box. The diffraction data of the benzene-methanol azeotrope show an increase in intensity at low values of the wavevector transfer, *Q*, with increasing scattering contrast. This observation already indicates the presence of local concentration fluctuations of benzene and methanol. The availability of three-dimensional structural models of the two azeotropes enables us to investigate their local structures in detail in the next step.

Local structure of the acetone-chloroform azeotrope

The local structure in liquids is governed by specific interactions which exist between neighbouring molecules. Attractive interactions between atoms of neighbouring molecules are typically revealed by close, sharp or intense features in intermolecular pair-correlation functions, $g_{ij}(r)$. These functions are obtained from the simulation boxes and reflect the probability of finding *j* type atoms as a function of the distance from an *i* type atom. The most likely interaction distance is indicated by a local maximum in these functions.

Figure 3 shows selected $g_{ij}(r)$s from the EPSR model of the acetone-chloroform azeotrope together with characteristic closest-approach distances of related crystalline materials.[45-47] The approximate interaction distances from EPSR models of the pure liquids are also included.[48, 49] Focussing on the O_A–H_C hydrogen bonding interaction, an important reference state is the 1:1 acetone-chloroform co-crystal formed at 150 K. In the co-crystal, the shortest O_A–H_C distance is 2.41 Å.[45] The maximum in the O_A–H_C $g_{ij}(r)$ at 2.76 Å indicates that the interaction distance in the azeotrope is significantly longer. However, the short distance in the co-crystal is achieved though positioning two chloroform and two acetone molecules in a specific bifurcated-dimer arrangement inhibiting several other close contacts. In particular, the H_C–Cl_C and O_A-$C1_A$ distances are much longer in the co-crystal than in the azeotrope, the pure liquid or crystalline reference states. The observed structural differences between the 150 K co-crystal and the room temperature liquid mixture are to be expected, as thermal energy destabilises any specific co-crystal structures and causes the system to explore its configurational manifold. Peaks at low *r* in the $g_{ij}(r)$s for O_A–Cl_C, H_C–Cl_C and Cl_C–Cl_C suggest that several charge-related interactions involving chlorine atoms are also important in the azeotrope. Indeed, distances in the azeotrope between these pairs are similar to those in the pure reference states. The peak in O_A–Cl_C is perhaps surprising given the negative partial charges of both atoms. However, the charge distribution about chlorine atoms is quadrupolar giving rise to a positively-charged distal terminus on the Cl atom,[50] which can then interact with negatively charged atoms such as O_A. Such an interaction, commonly referred to as halogen bonding,[51, 52] was postulated for co-crystals of chloroform and cyclobutanone,[45] and seems to be present in the acetone-chloroform azeotrope as well.

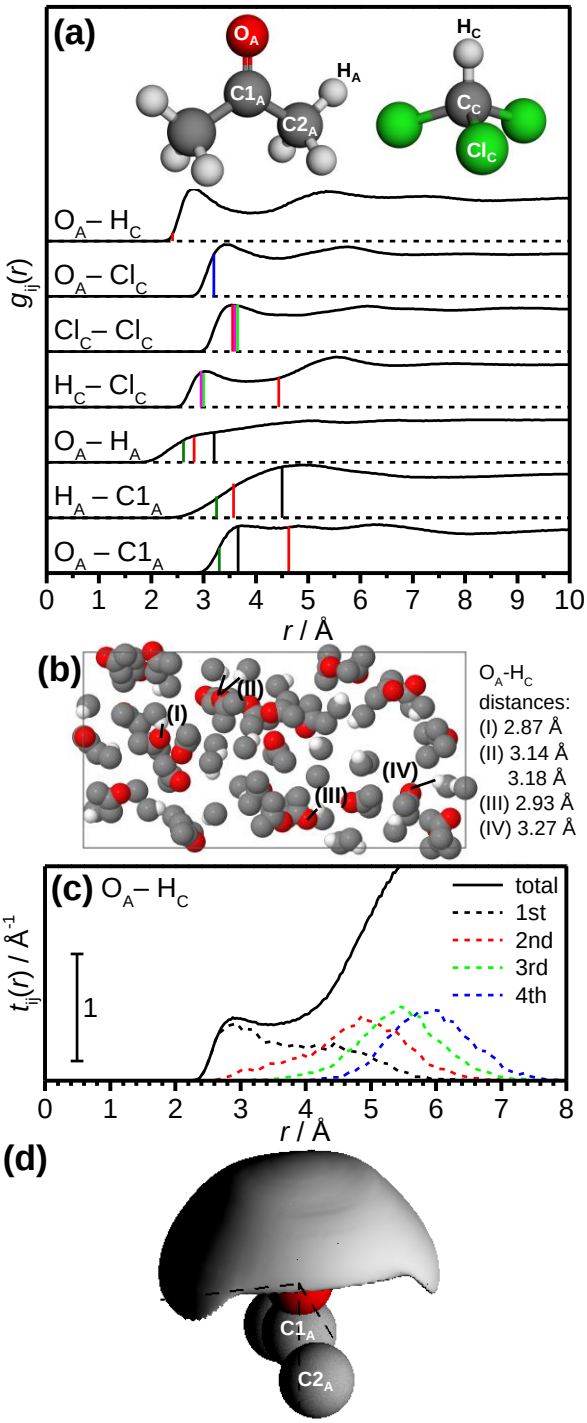

Figure 3 (a) Selected $g_{ij}(r)$ functions obtained from the EPSR model of the acetone-chloroform azeotrope. Tick marks indicate corresponding distances in the 1:1 acetone-chloroform cocrystal[45] (red), the 1:1 cyclobutanone-chloroform cocrystal[45] (blue), crystalline chloroform[46] (magenta), crystalline acetone[47] (dark green), liquid chloroform[49] (light green) and liquid acetone (black).[48] (b) A **1**0×20×10 Å slice of the EPSR simulation box showing the distances of several acetone-chloroform interactions (chlorine and methyl hydrogens are not shown). (c) O_A–H_C $t_{ij}(r)$ separated into contributions from 1st, 2nd, 3rd and 4th closest H_C neighbours using the ANGULA software.[53-56] (d) O_A–H_C spatial density function plotted in the 1 – 3.5 Å distance range with a fractional isosurface level of 0.4.

The nature of O_A–H_C hydrogen bonding interactions in the azeotrope is more closely examined in Figure 3(b,c) which

shows the range of different interaction structures in a randomly chosen 10×20×10 Å slice of the simulation box and the separation of the O_A–H_C $t_{ij}(r)$ pair-correlation function into contributions from 1st, 2nd, 3rd and 4th closest H_C atoms. The $t_{ij}(r)$ correlation function is calculated from $g_{ij}(r)$ according to $t_{ij}(r)=4\pi r^2\rho g_{ij}(r)$ which means that the area under $t_{ij}(r)$ equates to coordination numbers.[57] In Figure 3(b) the O_A–H_C distances of several 1:1 acetone-chloroform and a single 1:2 acetone-chloroform interactions are indicated. Integration of the $t_{ij}(r)$ in Figure 3(c) for closest H_C atoms (black dashed) between limits of 2.2 and 3.5 Å reveals that 44 % of the acetone molecules form at least one close O_A–H_C interaction. The $t_{ij}(r)$ for the 2nd closest H_C atoms (red dashed) also shows some intensity within these limits indicating that 7.5% of acetone molecules form two close contacts. This is significantly different to the values of 20 and 5%, respectively, which were derived by Apelblat *et al.* using thermodynamic excess quantities.[8] The average interaction distance in the EPSR model is also longer than found in the Monte Carlo simulation study of Kamath *et. al*. who used a scalable chloroform potential to reproduce the measured vapour pressure.[22] We tested the potentials used in their study as reference potentials for EPSR, but obtained a significantly poorer fit to our neutron diffraction data compared to using the empirical potentials.

Figure 3(d) shows the O_A–H_C spatial density function (SDF) which highlights the volume where the O_A–H_C pair-correlation function takes the highest values.[58, 59] In line with the previous analysis, a rather diffuse 'cap' is found on top of O_A which is consistent with a structurally quite disordered hydrogen bond.

The EPSR model suggests that a variety of interactions contribute to the thermodynamic state of the acetone-chloroform azeotrope. By comparing the structural model of the acetone-chloroform azeotrope with pure liquid chloroform,[49] the previously observed unusual shift of the C_C-H_C stretching mode towards higher wavenumbers upon addition of chloroform to liquids with proton acceptor character[29, 60-62] can now be better understood. This observation, which is the opposite of what might be expected for C–H···O hydrogen bond formation, is attributed to the disturbance of chloroform's self-association in the pure liquid. This effect may also explain the 'non-specific' dilution shift in the ^{1}H-NMR spectra of chloroform-acetone mixtures.[26]

Figure 4 shows a comparison of the percentages of chloroform molecules in chains with collinear dipole moments in the EPSR models of pure liquid chloroform[49] and the acetone-chloroform azeotrope. The greater number of chloroform molecules with a chain length of 1 (*i.e.* no chloroform-chloroform associations) and lower number of chloroform molecules with chain length > 1 in the azeotrope than in pure chloroform shows that the self-association of chloroform is significantly disrupted in the azeotrope.

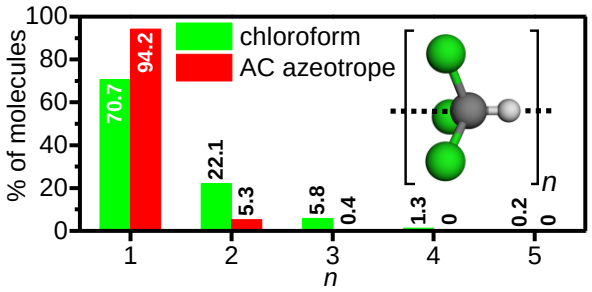

Figure 4 Chains analysis applied to the EPSR models of pure liquid chloroform[49] (green) and the acetone-chloroform azeotrope (red). Molecules were considered to be in a chain of chloroform molecules with collinear alignment of dipole moments for $r_{H\cdots C} < 4.2$ Å and $\gamma_{H\cdots C-H} > 150°$.

Local structure of the benzene-methanol azeotrope

A comparison of selected $g_{ij}(r)$s of the EPSR model of the benzene-methanol azeotrope with characteristic distances of the pure crystals[63, 64] and pure liquid methanol[37] are given in Figure 5(a). In contrast to acetone-chloroform, the $g_{ij}(r)$s of the benzene-methanol azeotrope indicate that the strength of the interactions between the components is substantially more unbalanced. The $g_{ij}(r)$s between methanol molecules are much more sharply defined at low r than those of benzene-benzene or benzene-methanol pairs. This is perhaps unsurprising given the polarity of methanol and its strong tendency to form hydrogen bonds.[34-38] Benzene-benzene and benzene-methanol interactions are clearly less specific in comparison.

The nature of the methanol-methanol interaction is more closely examined in Figure 5(b) which shows the O_M–O_M $t_{ij}(r)$ and its separation into contributions from 1st, 2nd, 3rd and 4th closest neighbours. The integration of $t_{ij}(r)$ for 1st and 2nd closest O_M neighbours using a conservative upper distance limit of 3.2 Å indicates that 88.4% of methanol molecules have at least one hydrogen bond (either donating or accepting) and 50.3% form two hydrogen bonds (both donating and accepting). Only about 5 % of methanol molecules form three hydrogen bonding interactions. The large proportion of methanol molecules in the azeotrope forming two hydrogen bonds suggests the formation of chains which enable the non-polar methyl groups to point outward towards less polar benzene-rich regions.

The local hydrogen-bonding environment of methanol is illustrated by the O_M–O_M SDF shown in Figure 5(c). Consistent with similar data presented for pure methanol,[37] the O_M atoms of neighbouring molecules are most likely found along the direction of the O_M–$H1_M$ bond, when the central molecule acts as a hydrogen bond donor, as well as below the O_M atom of the central molecule as it accepts hydrogen bonds from neighbouring molecules.

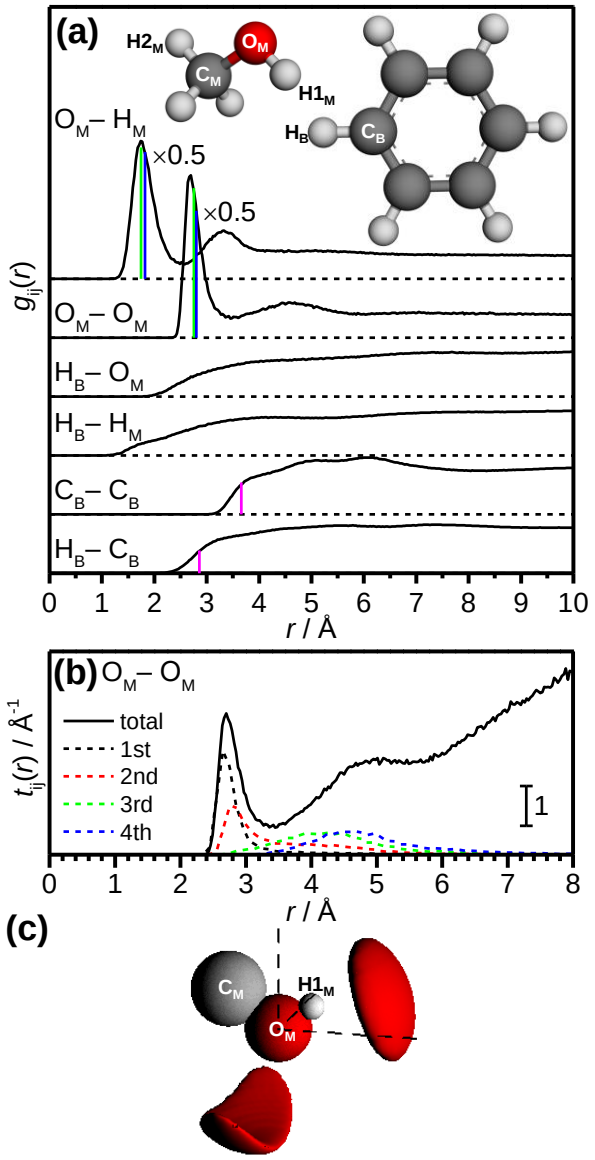

Figure 5 (a) Selected $g_{ij}(r)$ functions obtained from the EPSR model of the benzene-methanol azeotrope. Tick marks indicate corresponding distances in pure crystalline methanol (green)[65], pure crystalline benzene (magenta),[64] and liquid methanol (blue).[37] (b) O_M–O_M $t_{ij}(r)$ separated into contributions from 1st, 2nd, 3rd and 4th closest neighbours using the ANGULA software.[53-56] (c) O_M–O_M spatial density function plotted in the 1 – 3.2 Å distance range with a fractional isosurface level of 0.5.

Figure 6(a) shows the positions of OH head groups of methanol in a randomly chosen 20×40×10 Å slice of the simulation box. Figure 6(b) compares the proportion of methanol molecules forming chains containing between 1 (not forming a chain) and 20 molecules in the EPSR model of the azeotrope with the EPSR model of pure methanol at 25°C.[37] For consistency with the study on pure methanol, O_M–O_M and O_M–H_M distances of 3.4 Å and 2.4 Å were used as the upper limits to qualify methanol pairs as being hydrogen bonded. This analysis reveals that similar proportions of methanol molecules form chains in the azeotrope and in the pure liquid. However, significantly longer chains, $n > 6$, are found in the azeotrope suggesting that methanol is more structurally ordered in the azeotrope. This presumably reflects the much less satisfactory environment for short methanol chains in the benzene-containing azeotrope than in the generally more polar environments of pure liquid methanol. Figure 6(a) also illustrates that, in order to form such extensive chains, the two components of the azeotrope must begin to spatially separate locally. The chains in Figure 6(a) constitute methanol-rich regions and the empty spaces in between are packed with benzene molecules (omitted for clarity). This form of local separation is the consequence of the unbalanced strength of interactions in this azeotrope.

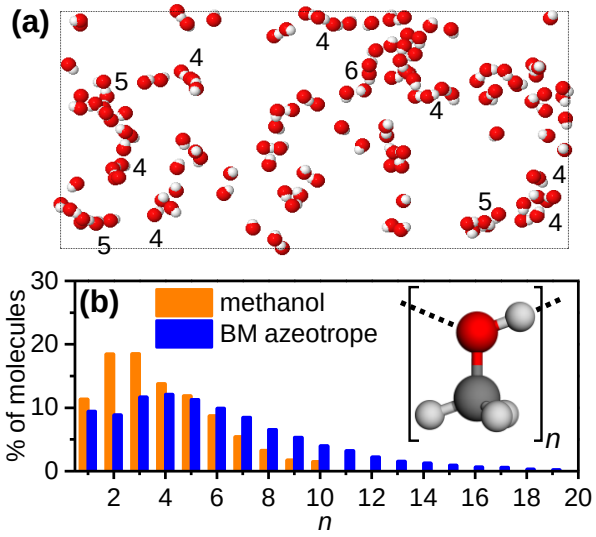

Figure 6 Methanol-methanol chain analysis. (a) Several methanol-methanol chains are highlighted in a 20×40×10 Å slice of the EPSR model of the benzene-methanol azeotrope. (b) A comparison of chain length distribution of the entire simulation box of the azeotrope and in the EPSR model of pure liquid methanol.[37]

Comparison of the local environments in the two different azeotropes

To compare the local environments of the two different types of azeotropes we classify the various local molecular environments according to the species that is most frequently found in the first coordination shell. So, for example, an *AC* environment denotes an acetone molecule whose first coordination shell contains more chloroform than acetone molecules. A full description of this structural classification scheme is provided in the ESI. The results of this analysis for the structural models of the two azeotropes are shown in Figure 7. The percentages of the local environments depend strongly on the relative strength of the interactions between like and unlike components but also on the overall composition of the mixture. It is therefore necessary to compare the percentages of the local environments from the structural models of the azeotropes with those expected for a corresponding random mixture of the same composition.

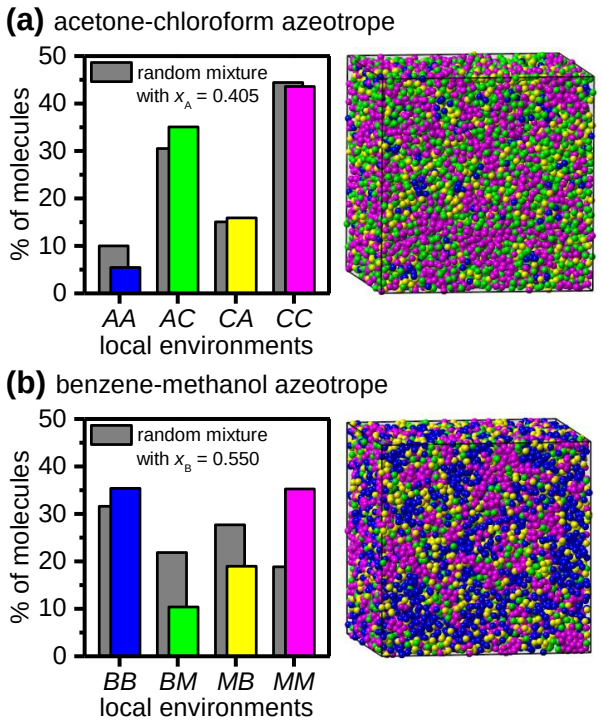

Figure 7 Classification of the local molecular environments in the two different azeotropes. The expected percentages of environments for the corresponding random mixtures are indicated by grey bars. The pictures of the simulation boxes show the spatial distributions of the various local environments using the same colour code as in the bar graph.

Larger percentages of *AC* and *CA* environments are found in the acetone-chloroform azeotrope compared to the corresponding random mixture which is consistent with the favourable interactions between acetone and chloroform molecules. The smaller decrease of *CC* environments compared to *AA* environments is in line with chloroform's tendency for self-aggregation into polar chains[49] which seems to be preserved to at least some extent in the azeotrope (*cf.* Figure 4).

The most striking deviation of the benzene-methanol azeotrope from the corresponding random mixture is found in the large percentages of *MM* environments. The less favourable interactions between benzene and methanol manifest in decreased amounts of *BM* and *MB* environments.

The emerging picture is that the more volatile components of both types of azeotropes, *i.e.* acetone and methanol (Figure 1), experience the more pronounced changes in their local environments as the azeotropes form. For the negative acetone-chloroform azeotrope this can be rationalised in the sense that the vapour pressure of the more volatile acetone needs to be reduced by a greater amount compared to chloroform in order to achieve the observed vapour-pressure depression. For the positive benzene-methanol azeotrope the unfavourable interactions between benzene and methanol drive the vapour pressure elevation. Since methanol is the more volatile component this effect needs to be counteracted more for methanol than for benzene through the more pronounced methanol-methanol interactions.

Analysis of long-range structure using Kirkwood-Buff integrals

In the next step we analyse the more long-range structures of the two azeotropes. For this, we use the centre-of-mass to centre-of-mass pair correlation functions, $g_{\mathrm{COM-COM}}(r)$, which contain information about the relative spatial arrangements of the molecules. The appearance of these functions reflects the size and composition of the molecular shells which exist in the azeotropes. Figure 8 shows that the three $g_{\mathrm{COM-COM}}(r)$ functions of the acetone-chloroform azeotrope are similar whereas for the benzene-methanol azeotrope they are significantly different. This reflects the differences in the partial molar volumes (V_A=122.7 Å^3 and V_C=133.7 Å^3; V_B=148.5 Å^3 and V_M=68.3 Å^3), the compositions of the molecular shells, as well as the overall nature of the packing.

The running Kirkwood-Buff integral, $G_{ij}(r_{max})$, is defined as $\int_0^{r_{max}} 4\pi r^2 (g_{\mathrm{COM-COM}}(r) - 1)\,\mathrm{d}r$.[40, 41, 66] This quantity therefore reflects the average deficiency or excess of species *j* with respect to the bulk average within the coordination shell of species *i* up to r_{max}. For a mixture of ideal gases $G_{ij}(r_{max})$ would be always zero and any deviation indicates non-ideality. Figure 8 shows the $G_{ij}(r_{max})$ functions of the two azeotropes calculated from the corresponding $g_{\mathrm{COM-COM}}(r)$ functions.

For the acetone-chloroform azeotrope the similar initial decrease in the three $G_{ij}(r_{max})$s between 0 and 4 Å reflects the excluded volume due to the size and shape of the molecules, and therefore the inherent deficiency of other molecules in this distance range. The oscillations that follow then accumulate differences in the local concentrations caused by attraction or repulsion between the components. The higher value of $G_{ij}(r_{max})$ for acetone-chloroform relative to the $G_{ij}(r_{max})$s of acetone-acetone and chloroform-chloroform reflects the favourable interactions between acetone and chloroform in the azeotrope. Above about 20 Å the $G_{ij}(r_{max})$s seem to converge to constant values indicating that the mixing of acetone and chloroform molecules is essentially random beyond this point.

The $G_{ij}(r_{max})$s of the benzene-methanol azeotrope look very different. The large intensity of the first peak in the methanol-methanol $g_{\mathrm{COM-COM}}(r)$, reflects the favourable methanol-methanol interactions and local excess of methanol, and gives rise to a positive feature between 4 and 20 Å in the $G_{ij}(r_{max})$. The $G_{ij}(r_{max})$ for benzene-methanol on the other hand shows a complementary feature of opposite sign indicating the corresponding local deficiency of benzene about methanol molecules and *vice versa*. The initially positive methanol-methanol feature is followed by a negative feature, indicating a region of deficiency. This is most likely linked with reaching the ends of the methanol-rich domains. The benzene-methanol $G_{ij}(r_{max})$ consequently gains intensity at around 20 Å. Unlike for the acetone-chloroform acetone the $G_{ij}(r_{max})$s of the benzene-methanol azeotrope do not converge to constant values within 60 Å, which is the maximum distance available from our simulation boxes.

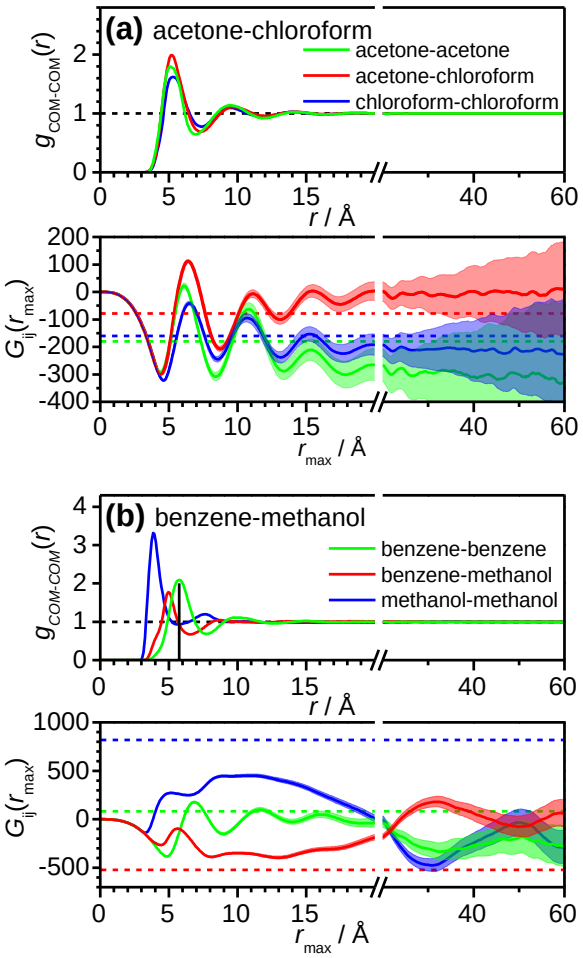

Figure 8 $g_{COM-COM}(r)$ and $G_{ij}(r_{max})$ functions of EPSR models of the (a) acetone-chloroform and (b) benzene-methanol azeotropes. The mean COM-COM distance from the EPSR model of the pure benzene[67] is indicated by a black line in (b). The dashed horizontal lines show the Kirkwood-Buff integrals calculated from thermodynamic data. The margins of error of the $G_{ij}(r_{max})$ functions are indicated by the shaded regions.

Running Kirkwood-Buff integrals have to converge eventually towards the Kirkwood-Buff integrals, G_{ij}s, at least as r_{max} tends to infinity.[19, 20, 38] Remarkably, these G_{ij}s provide a direct link between structural information and the thermodynamic properties of the liquid mixtures. In addition to estimating the G_{ij}s from the converged $G_{ij}(r_{max})$ functions, their values can be calculated from the molar volumes, isothermal compressibility and concentration dependence of the chemical potentials of the components in liquid mixtures.[19, 20, 38] The calculation of the G_{ij}s of the two azeotropes from thermodynamic data are provided as ESI and the obtained values are shown by dashed horizontal lines in Figure 8.

Encouragingly, the $G_{ij}(r_{max})$s of the acetone-chloroform azeotrope converge approximately to the values of the thermodynamic G_{ij}s. The small deviations may indicate that the attractive acetone-chloroform interaction is slightly overestimated and the attractive acetone-acetone interaction is slightly underestimated in the EPSR model. Equally, the differences could arise from small errors in the $g_{COM-COM}(r)$s which accumulate in the $G_{ij}(r_{max})$s.

For the benzene-methanol azeotrope, convergence of the $G_{ij}(r_{max})$s is not observed below 60 Å. We emphasise that this does not imply that the local or intermediate structures of the model are incorrect, only that the simulation box is not large enough to fully represent the long-range structure. The G_{ij} values calculated from thermodynamic data indicate where the oscillations are expected to converge in principle if a large enough simulation box were used. The close to zero G_{ij} for benzene-benzene pairs suggest that whilst methanol self-associates through hydrogen bonding interactions, the interaction between benzene molecules is much weaker. Consequently, the large G_{ij} for methanol-methanol requires a negative value for the benzene-methanol G_{ij}.

Conclusions

Our work gives new insight into the structure and properties of azeotropes. We have produced the first structural models of negative and positive azeotropes that are consistent with their experimental diffraction data. We have shown that mixing in negative and positive azeotropes is fundamentally different. There is intimate short-range mixing in the negative acetone-chloroform azeotrope and a tendency towards chain-like clustering of methanol in the positive benzene-methanol azeotrope. The emerging picture is that for both negative and positive azeotropes the more volatile components undergo the more pronounced changes in their local environments as the azeotropes form.

The more long-range structure of azeotropes is conveniently analysed with running Kirkwood-Buff integrals. For negative azeotropes we find good agreement between the Kirkwood-Buff integrals derived from our structural model and from thermodynamic data. This is consistent with the intimate molecular mixing at the local scale, which leads to convergence of the running Kirkwood-Buff integrals over the length scale of the simulation box. For the positive benzene-methanol azeotrope the more extended clustering of methanol means that much larger simulation boxes would be required to achieve convergence.

Our study provides a significant step forward towards linking the appearances of phase diagrams and other thermodynamic data with the microstructures of azeotropes. The ultimate aim will be to create specific molecular environments in azeotropes based on thermodynamic information in order to improve and fine-tune their performances.

Experimental

Acetone (CH_3COCH_3 and CD_3COCD_3), chloroform ($CHCl_3$ and $CDCl_3$), methanol (CH_3OH, CD_3OH and CD_3OD) and benzene (C_6D_6 and C_6H_6) were purchased from Sigma Aldrich, and used without further purification. Their quoted purities are >99.9 weight% and >99.96 D / H atom%. In total, 7 different isotopic mixtures of the acetone-chloroform and 10 different benzene-methanol mixtures were prepared at the azeotropic

compositions. Full details on the isotopic compositions of the various samples are given in the ESI.

For neutron scattering measurements the azeotropes were held in $Ti_{0.68}Zr_{0.32}$ null-scattering alloy sample cells with internal dimensions of 1×38×38 mm. The measurements were carried out on the Small Angle Neutron Diffractometer for Amorphous and Liquid Samples (SANDALS) and the Near and Intermediate Range Order Diffractometer (NIMROD) instruments at the ISIS spallation source at the Rutherford Appleton Laboratory, UK. The samples were maintained at 25°C during the measurements using an external water bath. Scattering data were collected for >1000 μA h of proton current per sample. Multiple scattering and inelasticity corrections were carried out using the GudrunN software package.[68]

The Empirical Potential Structural refinement (EPSR) software was used to fit the experimental data and to obtain structural models of the azeotropes. The EPSR calculations were carried on the UCL Chemistry departmental computer cluster. The ESI contains a description of the background theory on neutron diffraction including the isotopic substitution technique, details of the EPSR modelling including the molecular geometries as well as Lennard-Jones parameters and partial charges of the reference potential for the acetone, benzene, chloroform and methanol molecules. At least 1000 model iterations were accumulated to obtain structural information from the models. The EPSR subroutines SHARM and CHAINS were then used to extract the $g_{COM–COM}(r)$ and spatial density functions as well as chain-length distributions. The ANGULA software[53-56] was used to separate the $t_{ij}(r)$ functions into contributions from 1st, 2nd, 3rd and 4th closest neighbours. Our LENCA software was used to classify the local environments of the molecules in the simulation boxes. A full description of this approach is given in the ESI.

Acknowledgements

We thank ISIS for neutron beam time and a consumables grant, the Royal Society for a University Research Fellowship, D. Bowron for measuring samples via the NIMROD express route and for advice using EPSR with large simulation boxes, L. C. Pardo-Soto for help using his ANGULA software and J. Saßmannshausen for setting up EPSR on the UCL computer cluster.

References

1. W. Malesinski, *Azeotropy and Other Theoretical Problems of Vapour-Liquid Equilibrium*, John Wiley and Sons, New York, USA, 1965.
2. J. S. Rowlinson and F. L. Swinton, *Liquids and Liquid Mixtures*, Third edn., Butterworth Scientifics, London, 1982.
3. S. Widagdo and W. D. Seider, *AIChE J.*, 1996, **42**, 96-130.
4. V. N. Kiva, E. K. Hilmen and S. Skogestad, *Chem. Eng. Sci.*, 2003, **58**, 1903-1953.
5. *Handbook for Critical Cleaning: Cleaning agents and systems*, 2nd edn., CRC Books, Boca Raton, USA, 2011.
6. G. A. Busato and G. Bashein, *Update Anaesth.*, 2004, **18**, 1.
7. J. v. Zawidzki, *Z. Phys. Chem.*, 1900, **35**.
8. A. Apelblat, A. Tamir and M. Wagner, *Fluid Phase Eq.*, 1980, **4**, 229-255.
9. Y. Miyano and W. Hayduk, *J. Chem. Eng. Data*, 1993, **38**, 277-381.
10. L. Saroléa-Mathot, *Trans. Faraday Soc.*, 1953, **49**, 8-20.
11. A. N. Campbell and E. M. Kartzmark, *Can. J. Chem.*, 1960, **38**, 652-655.
12. E. R. Kearns, *J. Phys. Chem.*, 1961, **65**, 314-316.
13. K. W. Morcom and D. N. Travers, *Trans. Faraday Soc.*, 1965, **61**, 230-234.
14. T. Matsui, L. G. Hepler and D. V. Fenby, *J. Phys. Chem.*, 1973, **77**, 2397-2400.
15. K. Kojima, K. Tochigi, K. Kurihara and M. Nakamichi, *J. Chem. Eng. Data*, 1991, **36**, 343-345.
16. J. A. Hopkins, V. R. Bhethanabotla and S. W. Campbell, *J. Chem. Eng. Data*, 1994, **39**, 488-492.
17. V. A. Durov and I. Y. Shilov, *J. Chem. Soc. Faraday Trans.* , 1996, **92**, 3559-3563.
18. P. Oracz and S. Warycha, *Fluid Phase Equilib.*, 1997, **137**, 149-162.
19. S. Glasstone, *Trans. Faraday Soc.*, 1937, **33**, 200-206.
20. G. Scratchard, S. E. Wood and J. M. Mochel, *J. Am. Chem. Soc.*, 1946, **68**.
21. H. Toghiani, R. K. Toghiani and D. S. Viswanath, *J. Chem. Eng. Data*, 1994, **39**, 63-67.
22. G. Kamath, G. Georgiev and J. J. Potoff, *J. Phys. Chem. B*, 2005, **109**, 19463-19473.
23. J. R. Elliott and J. C. Rainwater, *Fluid Phase Equilibria*, 2000, **175**, 229-236.
24. C. M. Huggins, G. C. Pimentel and J. N. Shoolery, *J. Chem. Phys.*, 1955, **23**, 1244-1247.
25. R. Kaiser, *Can. J. Chem.*, 1963, **41**, 430-439.
26. K. Choi and D. W. Tedder, *AlChE J.*, 1997, **43**, 196-211.
27. M. R. Jalilian and L. Alibabaei, *Spectrochim. Acta Mol.*, 2005, **62**, 322-325.
28. T. S. Perova, D. H. Christensen and O. Faurskov Nielsen, *Vib. Spectrosc.*, 1997, **15**, 61-67.
29. P. D. Vaz, M. M. Nolasco, F. P. S. C. Gil, P. J. A. Ribeiro-Claro and J. Tomkinson, *Chem. Eur. J.*, 2010, **16**, 9010-9017.
30. G. S. Denisolv, *Opt. Spektrosk.*, 1961, **11**, 428.
31. Y. B. Monakhova, M. V. Pozharov, T. V. Zakharova, E. K. Khvorostova, A. V. Markin, D. W. Lachenmeier, T. Kuballa and S. P. Mushtakova, *J. Sol. Chem.*, 2014, **43**, 1963-1980.
32. N. Y. Tan, R. Li, P. Brauer, C. D'Agostino, L. F. Gladden and J. A. Zeitler, *Phys. Chem. Chem. Phys.*, 2015, **17**, 5999-6008.
33. M. R. Jalilian and S. F. Tayyari, *Spectrochim. Acta Mol.*, 2009, **73**, 828-832.
34. D. G. Montague, J. C. Dore and S. Cummings, *Mol. Phys.*, 1984, **53**, 1049-1066.
35. A. H. Narten and A. Habenschuss, *J. Chem. Phys.*, 1984, **80**, 3387-3391.
36. A. K. Karmakar, P. S. R. Krishna and R. N. Joarder, *Phys. Lett. A*, 1999, **253**, 207-210.
37. T. Yamaguchi, K. Hidaka and A. K. Soper, *Mol. Phys.*, 1999, **96**.
38. A. Sahoo, P. P. Nath, V. Bhagat, P. S. R. Krishna and R. N. Joarder, *Phys. Chem. Liq.*, 2010, **48**, 546-559.
39. E. A. Ploetz, N. Bentenitis and P. E. Smith, *J. Chem. Phys.*, 2010, **132**, 164501.
40. J. G. Kirkwood and F. P. Buff, *J. Chem. Phys.*, 1951, **19**, 774-777.

41. K. E. Newman, *Chem. Soc. Rev.*, 1994, **23**, 31-40.
42. A. Perera, F. Sokolic, L. Almasy and Y. Koga, *J. Chem. Phys.*, 2006, **124**, 124515.
43. A. K. Soper, *Chem. Phys.*, 1996, **202**, 295-306.
44. A. K. Soper, *Phys. Rev. B*, 2005, **72**, 104204.
45. D. S. Yufit and J. A. K. Howard, *CrystEngComm*, 2012, **14**, 2003-2008.
46. R. Fourme and M. Renaud, *C. R. Acad. Sci., Ser. C (Chim)*, 1966, **263**, 69.
47. D. R. Allan, S. J. Clark, R. M. Ibberson, S. Parson, C. R. Pulham and L. Sawye, *Chem. Comm.*, 1999, 751-752.
48. S. McLain, A. K. Soper and A. Luzar, *J. Chem. Phys.*, 2006, **124**, 074502.
49. J. J. Shephard, A. K. Soper, S. Imberti, J. S. O. Evans and C. G. Salzmann, *Chem. Comm.*, 2015, **51**, 4770-4773.
50. W. Zierkiewicz, R. Wieczorek, P. Hobza and D. Michalska, *Phys. Chem. Chem. Phys.*, 2011, **13**, 5105-5113.
51. P. Metrangolo and G. Resnati, eds., *Halogen Bonding*, Springer-Verlag, Heidelberg, 2008.
52. P. Politzer, J. S. Murray and T. Clark, *Phys. Chem. Chem. Phys.*, 2013, **15**, 11178.
53. L. C. Pardo, ANGULA Software Download, https://gcm.upc.edu/en/members/luis-carlos/angula/ANGULA, (accessed 1. 1. 2016, 2016).
54. L. C. Pardo, A. Henao and A. Vispa, *J. Non-Cryst. Solids*, 2015, **407**, 220-227.
55. L. C. Pardo, A. Henao, S. Busch, E. Guàrdia and J. L. Tamarit, *Phys. Chem. Chem. Phys.*, 2014, **16**, 24479-24483.
56. A. J. Johnston, S. Busch, L. C. Pardo, S. K. Callear, P. C. Biggin and S. E. McLain, *Phys. Chem. Chem. Phys.*, 2016, **18**, 991-999.
57. D. Keen, *J. Appl. Cryst.*, 2001, **34**, 172-177.
58. I. M. Svishchev and P. G. Kusalik, *J. Chem. Phys.*, 1993, **99**, 3049-3058.
59. C. G. Gray and K. E. Gubbins, *Theory of Molecular Fluids, Volume 1: Fundamentals*, Clarendon Press, Oxford, 1984.
60. A. Nikuradse, *Z. Phys. Chem.*, 1954, **2**, 9-24.
61. E. D. Becker, *Spectrochim. Acta*, 1959, **15**, 743-746.
62. P. J. A. Ribeiro-Claro and P. D. Vaz, *Chem. Phys. Lett.*, 2004, **390**, 358-361.
63. B. H. Torrie and S.-X. Weng, *Mol. Phys.*, 1989, **67**, 575.
64. G. A. Jeffrey, J. R. Ruble, R. K. McMullan and J. A. Pople, *Proc. Natl. Acad. Sci. Lond. A*, 1987, **414**, 47-56.
65. B. H. Torrie, O. S. Binbrek, M. Straussa and I. P. Swainson, *J. Solid State Chem.*, 2002, **166**, 415-420.
66. M. C. A. Donkersloot, *J. Sol. Chem.*, 1979, **8**, 293-307.
67. T. F. Headen, C. A. Howard, N. T. Skipper, M. A. Wilkinson, D. T. Bowron and A. K. Soper, *J. Am. Chem. Soc.*, 2010, **132**, 5735-5742.
68. A. K. Soper, *Mol. Phys.*, 2009, **107**, 1667-1684.